Design of a High-Performance Control Scheme for a Grid-Connected DFIG-Based Wind Energy Conversion System Using Model Predictive Control and Hysteresis Model

Zine Hamed Kamel Eddine*, Abed Khoudir
Department of Electrical Engineering, Faculty of Engineering Sciences, Mentouri University, Road Ain El Bey, Constantine, Algeria
kamel-eddine.zine-hamed@lec-umc.org; khoudir.abed@laposte.net

***Abstract*—In this paper, we present a novel design and development of wind energy conversion systems (WECS) for a doubly-fed induction generator (DFIG). A hysteresis current control is used to improve the DC bus for rectifier and smart current control by model predictive of three-level-NPC (3L-NPC) inverter. The advantages of this intelligent method are such as fast dynamic answers and the easy implementation of nonlinearities, and that it requires fewer calculations to choose the best switching state. In addition, an innovative algorithm is proposed to adjust the current ripples and output voltage harmonics of the wind energy conversion system. The performance of the system was analysed by simulation using MATLAB/Simulink.**

***Index Terms*—Doubly-fed induction generator; Hysteresis current control; Predictive current control; Wind energy conversion system; 3L-NPC.**

I. INTRODUCTION

Unlike conventional rectifiers, pulse width modulation (PWM) rectifiers are made using semiconductors controlled on opening and closing. The possibility of opening control allows full control of the converter because the switches can be switched, as required, both on closing and opening with a fairly high frequency. There are two ways to implement rectifiers: as current source rectifier and voltage source rectifier; traditional rectification technology is an uncontrolled rectification circuit composed of diodes. Its harm is to produce a large number of current harmonics and inject them into the grid, thus affecting the quality of power and reducing the service life of electronic equipment. Therefore, in recent years, single-phase PWM rectifiers have been extensively utilised in renewable energy generation [1], [2], motor drive systems, uninterruptible power supplies, and battery energy storage systems. A single-phase PWM rectifier has a higher power factor and lower harmonics compared to an uncontrolled rectifier [3].

Global energy consumption continues to increase, and the large part of this consumable energy comes from fossil fuels (oil, natural gas, coal, etc.), the massive use of which can lead to the depletion of these reserves and really threatens the environment.

Wind energy is clean and renewable energy, unlike conventional energy, which presents the constraints of distance from the electricity network and the constraints of fuel transport, as well as the periodic maintenance of the installations.

The problem with the multilevel inverters connected to the grid is its switching frequency, which is the main cause of harmonics and switching losses there due to a reduction in the efficiency of the inverter. The authors have investigated the possible technical impacts in voltage regulation, active and reactive power variations, transformer loading, current and voltage harmonics caused by the integration of renewable energy [4]–[6].

When trying to solve harmonic problems, more researchers used the sinusoidal pulse width modulation (SPWM) approach and implemented in wind energy conversion systems to lower the harmonic content on the output voltage waveform [7]. The space vector modulation (SVM) technique has remarkable performance in three-level-PWM topologies [8]. Other techniques involving modulation methods at a low switching frequency that have attained more demand in a broader field of function are Staircase modulation, selective harmonic elimination (SHE) [9], [10], space vector control (SVC) [11], and sliding mode control (SMC) for doubly-fed induction generator (DFIG) [12].

This work proposes a new smart current control that is based on utilising predictive current control of three-level-NPC (3L-NPC) inverter by wind energy conversion systems (WECS) connected to grid-based DFIG and a hysteresis current controlled rectifier capable of handling these problems: the influence of harmonic disturbances (similar current total harmonic distortion (THD)), voltage stress, switching losses, rise time, overshoot, undershoot, and settling time of WECS.

The basic idea of this control is to choose the best switching state of the power switches with the switching state that minimises the quality function, selected of the order predictive current control of WECS for the continual increase in the power transmitted to the electrical grid while ensuring

Manuscript received 14 May, 2023; accepted 25 September, 2023.

reduction of current ripples and output voltage harmonics.

The organization of the rest of this paper is as follows. The configuration of the application generator, the turbine modelling, the multiplier modelling, and the DFIG modelling are presented in Section II. The hysteresis current control rectifier, modelling of the rectifier, functional representation of the PWM rectifier in the three-phase and PWM to hysteresis band are shown in Section III. The three-level-NPC inverter with predictive current control implementation, the 3L-NPC model inverter, the predictive current control implementation, and the cost function are discussed in Section IV. Simulation results studies are presented and discussed in Section V. Comparison to the state of the art is summarised in Section VI. The conclusions are provided in Section VII.

II. CONFIGURATION FOR APPLICATION GENERATOR

In this drive system, we are interested in the wound rotor doubly-fed induction generator (DFIG) and its use for the production of electrical energy from wind power. DFIG with double power supply with dissipated rotor energy: this variable speed configuration is represented in Fig. 1.

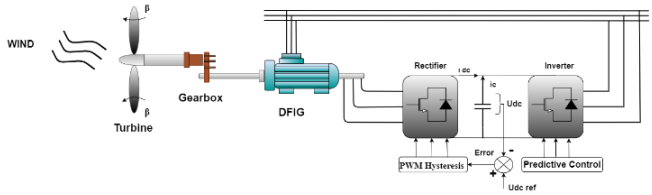

Fig. 1. DFIG-based wind energy conversion system.

The stator is connected directly to the network, and the rotor is connected to a rectifier (rotor side converter). Predictive control is applied to an inverter 3L-NPC (grid side converter) that is placed on the output of the rectifier controlled by PWM hysteresis.

A. Turbine Modelling

The modelling of the turbine consists in expressing the extractable power as a function of the wind speed and the operating conditions; this makes it possible to know the wind torque applied to the wind turbine. This modelling is based on bibliographic cross-checking or additional information from brochures from different manufacturers [13]

$$P_{aer} = \frac{1}{2} C_P(\lambda, \beta) \rho S V_V^3 = \frac{1}{2} \rho \pi R_T^2 V_V^3, \quad (1)$$

with

$$\lambda = \frac{\Omega_T R_T}{V_V}, \quad (2)$$

where λ is the speed ratio (rad), β depicts the angle of the blades of the orientation, Ω_T is the turbine rotation speed, R_T represents length (radius) of the blade, V_V represents the wind speed, and ρ is the density of the air (1.22 kg/m^3 at atmospheric pressure at 15 °C).

The Betz limit is that the power coefficient Cp (λ, β) does not exceed the value 16/17 = 0.59 [13], [14].

B. Multiplier Modelling

The turbine speed must be adjusted to the generator speed (DFIG). For this, we grant a multiplier between the turbine and the DFIG, the latter is mathematically modelled by the following equations:

$$C_g = \frac{C_T}{G}, \quad (3)$$

and

$$\Omega_T = \frac{\Omega_{mec}}{G}. \quad (4)$$

The mechanical equation:

$$\frac{C_T}{G} - C_g = \left(\frac{J_T}{G^2} + J_g\right)\frac{d\Omega_{mec}}{dt} + \left(\frac{f_T}{G} + f_g\right)\Omega_{mec}, \quad (5)$$

$$\frac{J_T}{G^2} + J_g = J, \quad (6)$$

$$\frac{f_T}{G} + f_g = f. \quad (7)$$

So, the mechanical equation will be like this:

$$C_{mec} = J\frac{d\Omega_{mec}}{dt}, \quad (8)$$

$$C_{mec} = C_g - C_{em} - C_{vis}, \quad (9)$$

$$C_{vis} = f\Omega_{mec}. \quad (10)$$

C_T, C_g, C_{vis} are the wind couple, the electromagnetic couple, and the viscous couple, respectively. J_T and J_g represent the inertia of the turbine and that of the generator, f_T and f_g are the coefficient of viscous friction of the turbine and that of the generator, G represents the ratio of the speed multiplier, and Ω_{mec} is the generator rotation speed (fast axis).

C. DFIG Modelling

Therefore, the DFIG mathematical model is written in Park's frame of reference linked to the field turn as follows [14], [15].

The equations of tensions:

$$\begin{cases} V_{ds} = R_s I_{ds} + \dfrac{d\varphi_{ds}}{dt} - \omega_s \varphi_{qs}, \\ V_{qs} = R_s I_{qs} + \dfrac{d\varphi_{qs}}{dt} + \omega_s \varphi_{ds}, \\ V_{dr} = R_r I_{dr} + \dfrac{d\varphi_{dr}}{dt} - (\omega_s - \omega)\varphi_{qr}, \\ V_{qr} = R_r I_{qr} + \dfrac{d\varphi_{qr}}{dt} - (\omega_s - \omega)\varphi_{dr}, \\ J\dfrac{d\Omega_r}{dt} = C_{em} - C_r - f_r\Omega_r. \end{cases} \quad (11)$$

The equations of the fields:

$$\begin{cases} \varphi_{ds} = L_s I_{ds} + M I_{dr}, \\ \varphi_{qs} = L_s I_{qs} + M I_{qr}, \\ \varphi_{dr} = L_r I_{dr} + M I_{ds}, \\ \varphi_{qr} = L_r I_{qr} + M I_{qs}, \end{cases} \tag{12}$$

$$C_{em} = \frac{M}{L_r} p\left(\varphi_{dr} I_{qs} - \varphi_{qr} I_{ds}\right). \tag{13}$$

The electromagnetic couple becomes

$$C_{em} = \frac{3}{2}\frac{M}{L_s} p\left(\varphi_{qs} I_{rd} - \varphi_{sd} I_{rq}\right). \tag{14}$$

The active and reactive powers of the stator and rotor are expressed by

$$\begin{cases} P_s = \frac{3}{2}\left(V_{ds} I_{ds} + V_{qs} I_{qs}\right), \\ Q_s = \frac{3}{2}\left(V_{qs} I_{ds} + V_{ds} I_{qs}\right), \\ P_r = \frac{3}{2}\left(V_{dr} I_{dr} + V_{qr} I_{qr}\right), \\ Q_r = \frac{3}{2}\left(V_{qr} I_{dr} + V_{dr} I_{qr}\right). \end{cases} \tag{15}$$

R_s, R_r are stator and rotor resistances, L_s, L_r, and M are stator, rotor, and mutual inductances, respectively, I_{ds}, I_{qs}, I_{dr} , and I_{qr} represent stator and rotor currents in the d-q frame, P_s, Q_s, P_r, and Q_r represent stator and rotor active and reactive powers, V_{ds}, V_{qs}, V_{dr}, and V_{qr} represent stator and rotor voltage components in the d-q frame, ω_s is the speed of stator magnetic field. $\omega_r = \omega_s - \omega$ is the angular speed of rotor.

III. HYSTERESIS CURRENT CONTROL RECTIFIER

A. Rectifier Modelling

The rectifier bridge consists of three arms with six bipolar transistors antiparallel with diodes. These switches are controlled by closing and opening (pulse time closing "0" and opening "1"). And in the same arm, the switches operate in a complementary way ($K_a = \overline{K_a'}$) to avoid the short circuit [16], [17]. The bridge rectifier model is depicted in Fig. 2.

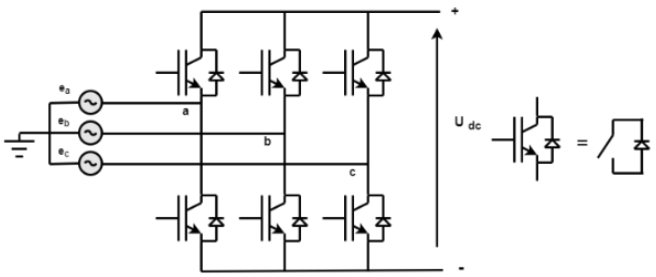

Fig. 2. Bridge rectifier.

The different switching and combination states of the PWM rectifier switches are shown in Table I.

From this table we can represent rectifier input voltages in general as follows [18], [19]:

$$V_{ab} = \left(S_a - S_b\right)U_{dc}, \tag{16}$$

$$V_{bc} = \left(S_b - S_c\right)U_{dc}, \tag{17}$$

$$V_{ca} = \left(S_c - S_a\right)U_{dc}. \tag{18}$$

From which we can deduce the phase-to-neutral voltages:

$$V_b = f_b U_{dc}, \tag{19}$$

$$V_c = f_c U_{dc}, \tag{20}$$

with:

$$f_a = \frac{2S_a - \left(S_b + S_c\right)}{3}, \tag{21}$$

$$f_b = \frac{2S_b - \left(S_a + S_c\right)}{3}, \tag{22}$$

$$f_c = \frac{2S_c - \left(S_a + S_b\right)}{3}. \tag{23}$$

TABLE I. THE EIGHT POSSIBLE STATES OF THE SWITCHES.

K	Sa	Sb	Sc	Vab	Vbc	Vac
0	1	0	0	Udc	0	-Udc
1	1	1	0	0	Udc	-Udc
2	0	1	1	-Udc	Udc	0
3	0	1	0	-Udc	0	Udc
4	0	0	1	0	-Udc	Udc
5	1	0	1	Udc	-Udc	0
6	0	0	0	0	0	0
7	1	1	1	0	0	0

The eight possible states of the input voltage V in a complex plane α β [20]:

$$V_{k+1} = \begin{cases} \left(\frac{2}{3}\right) U_{dc} e^{\frac{jk\pi}{3}} \xrightarrow{for} k = 0 \ldots 5. \\ V_7 = V_0 = 0 \end{cases} \tag{24}$$

The eight voltage vectors noted as V0 (0 0 0)-V7 (1 1 1) are presented in Fig. 3.

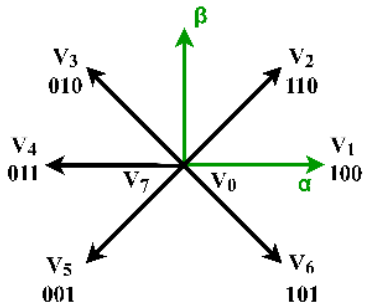

Fig. 3. Presentation of the voltage vector V_k.

B. Functional Representation of the PWM Rectifier in the Three-Phase Reference

The voltage equations for the balanced three-phase system without neutral can be written as (Fig. 3):

$$\bar{e} = \bar{V}_1 + V, \tag{25}$$

$$\bar{e} = R\bar{i} + L\frac{d\bar{i}}{dt} + \bar{V}, \tag{26}$$

$$\begin{bmatrix} e_a \\ e_b \\ e_c \end{bmatrix} = R\begin{bmatrix} i_a \\ i_b \\ i_c \end{bmatrix} + L\frac{d}{dt}\begin{bmatrix} i_a \\ i_b \\ i_c \end{bmatrix} + \begin{bmatrix} V_a \\ V_b \\ V_c \end{bmatrix}. \quad (27)$$

And the rectifier input voltage can be written as follows

$$V_n = U_{dc}\left(S_n \frac{1}{3}\sum_{n=a}^{c} S_n\right), \quad (28)$$

where S_n = 0 or 1 is the state of the switches, where (n = a, b, c). In addition, we can write the DC bus current as

$$C\frac{dU_{dc}}{dt} = i_c. \quad (29)$$

The current in the capacitor can be also written:

$$i_c = i_{dc} - i_{ch}, \quad (30)$$

$$C\frac{dU_{dc}}{dt} = S_a i_a + S_b i_b + S_c i_c - i_{dc}. \quad (31)$$

Also, the current i_c is the sum of the product of the currents of each phase by the state of its switch [16]

$$C\frac{dU_{dc}}{dt} = S_a i_a + S_b i_b + S_c i_c - i_{ch}. \quad (32)$$

So, the AC side of the rectifier:

$$L\frac{di_a}{dt} + Ri_a = e_a - U_{dc}\left(S_a - \frac{1}{3}\sum_{n=a}^{c} S_n\right) = e_a - \\ -U_{dc}\left(S_a - \frac{1}{3}(S_a + S_b + S_c)\right), \quad (33)$$

$$L\frac{di_b}{dt} + Ri_b = e_b - U_{dc}\left(S_b - \frac{1}{3}\sum_{n=a}^{c} S_n\right) = e_b - \\ -U_{dc}\left(S_b - \frac{1}{3}(S_a + S_b + S_c)\right), \quad (34)$$

$$L\frac{di_c}{dt} + Ri_c = e_c - U_{dc}\left(S_c - \frac{1}{3}\sum_{n=a}^{c} S_n\right) = e_c - \\ -U_{dc}\left(S_c - \frac{1}{3}(S_a + S_b + S_c)\right), \quad (35)$$

where the network voltages are expressed by:

$$e_c = E_m sin(\omega t), \quad (36)$$

$$e_b = E_m sin\left(\omega t - \frac{2\pi}{3}\right), \quad (37)$$

$$e_c = E_m sin\left(\omega t - \frac{2\pi}{3}\right). \quad (38)$$

The above equation can be summarised as follows:

$$L\left(\frac{d}{dt} + R\right)i_n = e_n - U_{dc}\left(S_n - \frac{1}{3}\sum_{n=a}^{c} S_n\right), \quad (39)$$

$$C\frac{dU_{dc}}{dt} = \sum_{k=a}^{c} i_n S_n - i_{ch}. \quad (40)$$

C. PWM to Hysteresis Band

The purpose of the hysteresis controller is to force the actual current to follow the predefined reference current. In conventional hysteresis controller, the comparators switch between the fixed bandwidths; this technique only requires a hysteresis comparator per phase [21], [22].

The principle of hysteresis used in this system is expressed in Fig. 4; the switch opens if the error becomes less than –H/2, it closes if the latter is greater than +H/2, where H represents the range (or width) of hysteresis. If the error is now between –H/2 and +H/2, (it varies within the hysteresis range), the switch does not switch [21], [23].

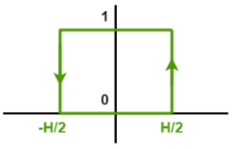

Fig. 4. Diagram of the proposed hysteresis controller.

The topology of the PWM technique used in the hysteresis current control in this configuration is shown in Fig. 5.

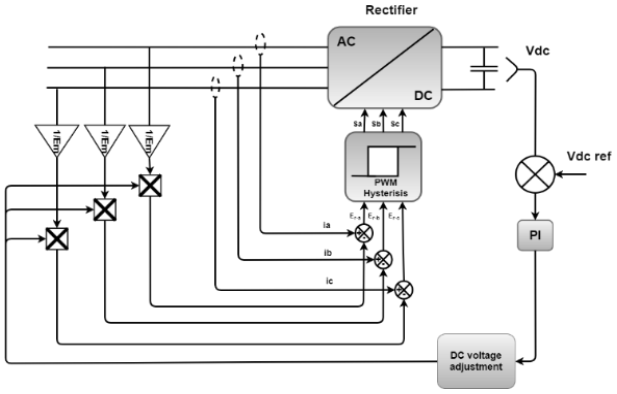

Fig. 5. Control diagram of the rectifier for the hysteresis current control connected to the inverter.

IV. IMPLEMENTATION PREDICTIVE CURRENT CONTROL THREE-LEVEL-NPC INVERTER

A. Inverter 3L-NPC Modelling

The power and control circuit of a three-level-NPC inverter connected to the grid is shown in Fig. 6, each phase of the three-phase three-level-NPC inverter consists of three arms composed of four switches (S1, S2, S3, and S4) connected in series and two median diodes (D1 and D2). The midpoints of the switches (S2 and S3) of each phase are connected to the load and the midpoints of the diodes (D1 and D2) are connected to the NP [24], [25].

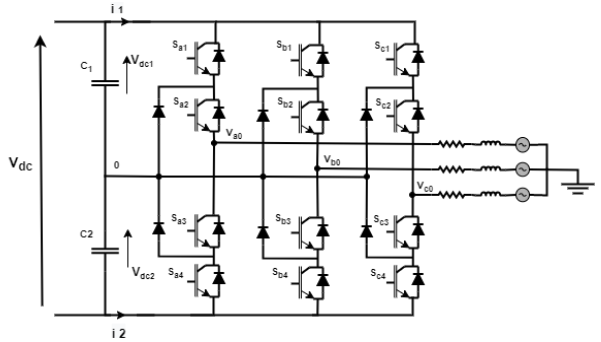

Fig. 6. Model of the power circuit of a three-level-NPC inverter connected to the grid.

In the same arm, the switches operate in a complementary way. The connection functions of the arm switches k (a complementary way) will be given by:

$$\begin{cases} \begin{cases} S_{a1} = \overline{S_{a2}}, \\ S_{a3} = \overline{S_{a4}}, \end{cases} \\ \begin{cases} S_{a1} = \overline{S_{a3}}, \\ S_{a2} = \overline{S_{a4}}, \end{cases} \\ \begin{cases} S_{a1} = \overline{S_{a4}}, \\ S_{a2} = \overline{S_{a3}}. \end{cases} \end{cases} \tag{41}$$

The switching function on the a, b, and c phase can be defined as follows:

$$\begin{cases} \begin{cases} S_{k1} = \overline{S_{k3}}, \\ S_{k2} = \overline{S_{k4}}, \end{cases} \\ \begin{cases} S_{k1} = 1 - S_{k3}, \\ S_{k2} = 1 - S_{k4}. \end{cases} \end{cases} \tag{42}$$

The equations of voltages (a), (b), (c) of the three-level inverter, with respect to the midpoint "0" of the input voltage source, are expressed as [26], [27]:

$$\begin{cases} v_{ao} = \left(S_{a1}S_{a2} - S_{a3}S_{a4}\right)V_{dc}, \\ v_{bo} = \left(S_{b1}S_{b2} - S_{b3}S_{b4}\right)V_{dc}, \\ v_{co} = \left(S_{c1}S_{c2} - S_{c3}S_{c4}\right)V_{dc}. \end{cases} \tag{43}$$

Compound voltages in matrix form are

$$\begin{bmatrix} v_{ab} \\ v_{bc} \\ v_{ac} \end{bmatrix} = \begin{bmatrix} v_{ao} - v_{bo} \\ v_{bo} - v_{co} \\ v_{ao} - v_{co} \end{bmatrix} = \\ = \begin{bmatrix} 1 & -1 & 0 \\ 0 & 1 & -1 \\ -1 & 0 & 1 \end{bmatrix} \begin{bmatrix} S_{a1}S_{a2} - S_{a3}S_{a4} \\ S_{b1}S_{b2} - S_{b3}S_{b4} \\ S_{c1}S_{c2} - S_{c3}S_{c4} \end{bmatrix}. \tag{44}$$

We can define the simple voltages (v_a, v_b, v_c) with respect to the neutral point *n:*

$$\begin{cases} v_a = v_{an} = v_{ao} - v_{no}, \\ v_b = v_{bn} = v_{bo} - v_{no}, \\ v_c = v_{cn} = v_{ao} - v_{no}. \end{cases} \tag{45}$$

The voltage equation between the midpoint of the DC power supply of the inverter and the point load neutral is written as follows

$$v_{no} = \frac{1}{3}\left(v_{ao} + v_{bo} + v_{co}\right). \tag{46}$$

Finally, the system in matrix form is presented as

$$\begin{bmatrix} v_a \\ v_b \\ v_c \end{bmatrix} = \frac{1}{3}\begin{bmatrix} 2 & -1 & -1 \\ -1 & 2 & -1 \\ -1 & -1 & 2 \end{bmatrix} \begin{bmatrix} S_{a1}S_{a2} - S_{a3}S_{a4} \\ S_{b1}S_{b2} - S_{b3}S_{b4} \\ S_{c1}S_{c2} - S_{c3}S_{c4} \end{bmatrix} V_{dc}. \tag{47}$$

B. Implementation Predictive Current Control

The proposed predictive control strategy is based on the fact that only a finite number of possible switching states can be generated by a static power converter and that models of the system can be used to predict behaviour variables for each switching state. To apply the appropriate selection by switching, a selection criterion must be defined. This selection criterion is expressed as a quality function that will be evaluated for the variables of predicted values to control. The prediction of the future value of these variables is calculated for each possible switching state. The switching state that minimises the quality function is selected [28], [29]. This approximation is considered in Fig. 7.

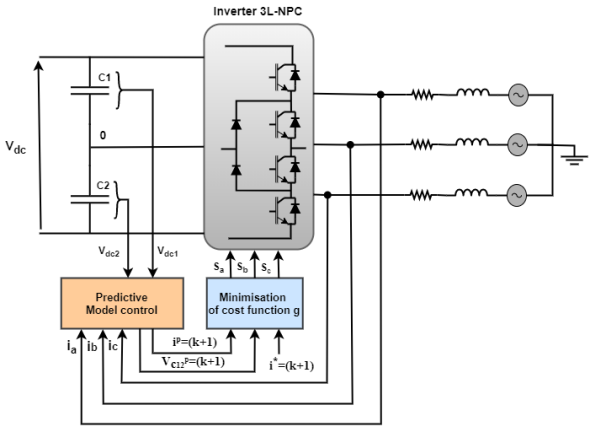

Fig. 7. Block diagram of predictive current control for a three-level-NPC inverter connected to the grid.

The system model equations are given as follows:

$$\begin{cases} V_{an} = Ri_a + L\dfrac{di_a}{dt} - e_a, \\ V_{bn} = Ri_b + L\dfrac{di_b}{dt} - e_b, \\ V_{cn} = Ri_c + L\dfrac{di_c}{dt} - e_c. \end{cases} \tag{48}$$

After the Clarke transformation and with the use of Euler's method to obtain a discrete-time model of the current, the current equations is expressed as follows

$$\frac{di}{dt} = \frac{i(k+1) - i(k)}{T_S}. \tag{49}$$

T_S is the sampling period and k shows sampling time.

$$\begin{cases} i_\alpha^p(k+1) = \left(1 - T_S\dfrac{R}{L}\right)i_\alpha(k) + \dfrac{T_S}{L}\left(v_\alpha - e_\alpha(k)\right), \\ i_\beta^p(k+1) = \left(1 - T_S\dfrac{R}{L}\right)i_\beta(k) + \dfrac{T_S}{L}\left(v_\beta - e_\beta(k)\right). \end{cases} \tag{50}$$

The currents (i_{c1}, i_{c2}) supplied by each capacitor (C_1, C_2) are represented by the following equations:

$$\begin{cases} i_{c1}(k) = i_{dc}(k) - H_{1a}i_a(k) - H_{1b}i_b(k) - H_{1c}i_c(k), \\ i_{c2}(k) = i_{dc}(k) + H_{2a}i_a(k) + H_{2b}i_b(k) + H_{2c}i_c(k). \end{cases} \quad (51)$$

The switch states function of the 3L-NPC calculates the variables (H_{1X}, H_{2X}) and are given by:

$$\begin{cases} H_{1X} = \begin{cases} 1 \; if \; S_X = "+", \\ 0 \; other, \end{cases} \\ H_{2X} = \begin{cases} 1 \; if \; S_X = "-", \\ 0 \; other. \end{cases} \end{cases} \quad (52)$$

We use the Euler method to obtain the equations in discrete time, which allows the prediction of DC bus voltages as follows:

$$\begin{cases} v_{c1}^p(k+1) = v_{c1}(k) + \frac{1}{C} i_{c1}(k) T_S, \\ v_{c2}^p(k+1) = v_{c2}(k) + \frac{1}{C} i_{c2}(k) T_S. \end{cases} \quad (53)$$

C. Cost Function

The objective of the current control scheme is to minimise the error between the measured currents and the reference values. This requirement can be written as a cost function. The cost function is expressed in orthogonal coordinates and measures the error between the references and the predicted currents

$$g = \left|i_\alpha^* - i_\alpha^p\right| + \left|i_\beta^* - i_\beta^p\right| + \lambda_{dc}\left|v_{c1}^p - v_{c2}^p\right|, \quad (54)$$

where λ_{dc} represent the weighting factor. The evaluation of the precomputed results and the determination of future optimal control actions are made by the cost function [30], [31].

V. Simulation Results and Discussion

This section is to validate the results obtained from the smart predictive current control model of the three-level-NPC inverter algorithm of WECS through eigenvalue analysis and also the comparative studies between the proposed model and the existing solution already used for DFIG connected to the grid.

In the first part, the results obtained after rotor side converter are illustrated in Fig. 8.

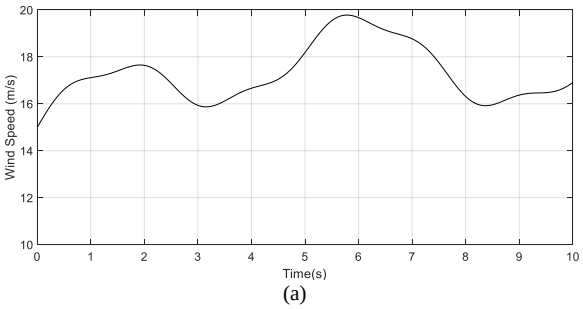

(a)

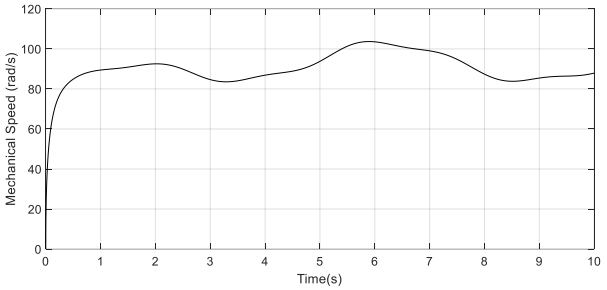

(b)

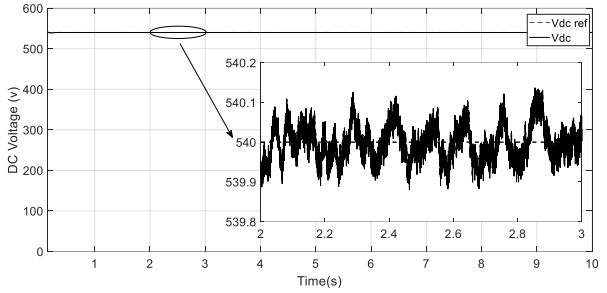

(c)

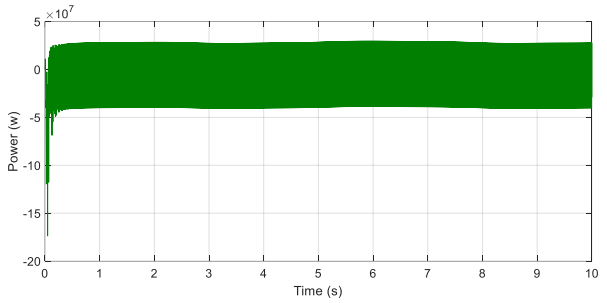

(d)

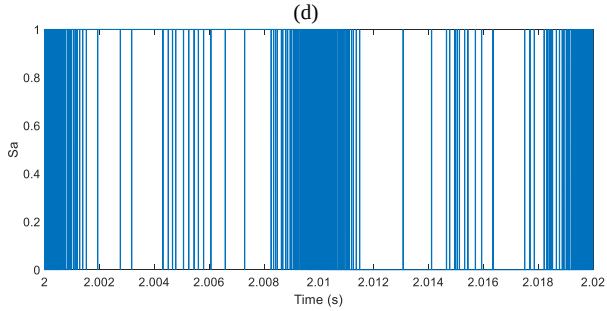

(e)

Fig. 8. Simulation results of the rotor side converter: (a) Wind speed (m/s); (b) Mechanical speed (rad/s); (c) DC link voltage (v); (d) DFIG active power (w); (e) Control Sa.

Figure 8(a) shows the variable change applied to the wind profile for the system studied.

Figure 8(c) presents the form of the DC link voltage. The DC link voltage reference is set to 540 V, the measured voltage perfectly follows the reference signal.

The second part shows the results after grid side converter, and are illustrated in Fig. 9.

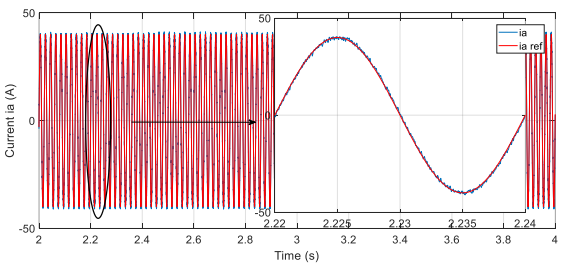

(a)

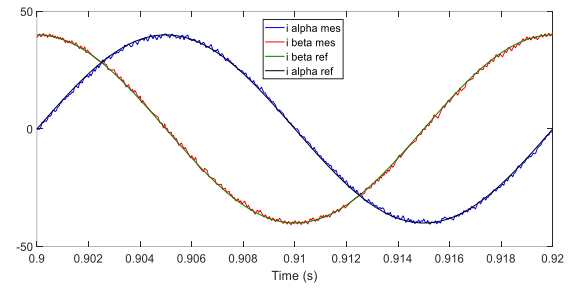

(b)

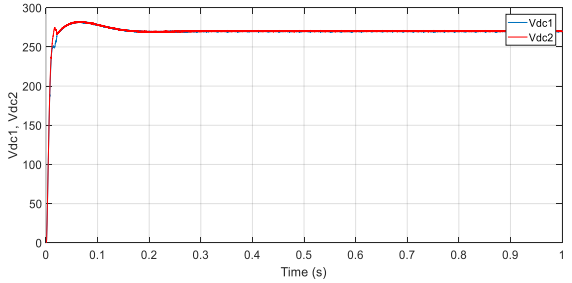

(c)

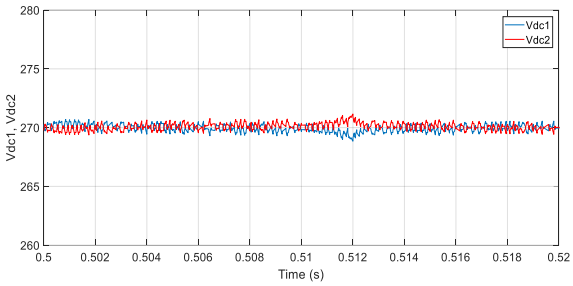

(d)

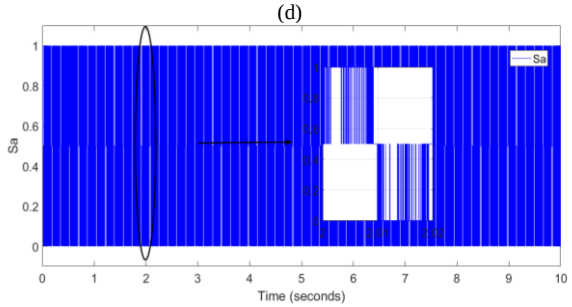

(e)

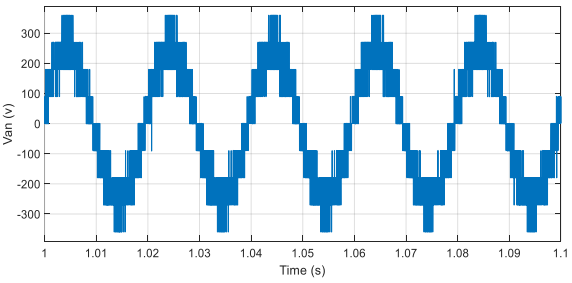

(f)

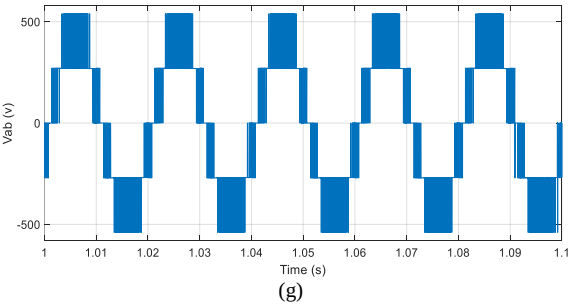

(g)

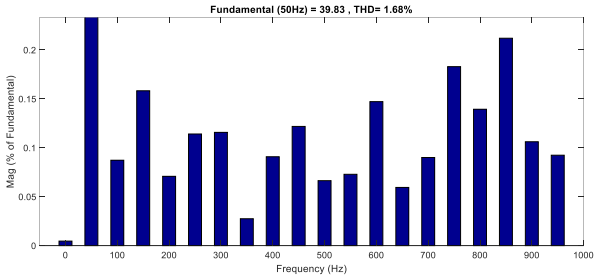

(h)

Fig. 9. Simulation results of the grid side converter: (a) Output current ia (A); (b) The controlled currents i_α (A) and i_β (A), as well as their references; (c) DC voltages across the two capacitors Vdc1, Vdc2 (v), (d) Zoom of the DC voltages across the two capacitors Vdc1, Vdc2; (e) Control Sa; (f) The simple voltage at inverter output Van (v); (g) Output line-to-line voltage Vab (v); (h) Spectrum of current ia.

Figure 9(a) clearly shows the proper tracking of the converter reference currents with small current ripples.

It can be seen from Fig. 9(b) that the waveform of the controlled currents i_α and i_β is smooth and stable.

Figure 9(c) illustrates that the DC voltage ripples are low enough.

The spectral analysis of the modulated voltage signal is presented in Fig. 9(h), where we noticed a drop in THD.

VI. COMPARISON TO THE STATE OF THE ART

The objective in this part is a comparative study between the smart current control of the WECS and the existing solution used in [10].

Finally, a comparative analysis of the existing solution [10] and the new WECS smart current control in terms of implementation is shown in Table II.

TABLE II. COMPARATIVE ANALYSIS OF SMART CURRENT CONTROL AND EXISTING SOLUTION.

	Existing solution [10]	**Smart current control**
Answer dynamic	Good	High
The behaviour of current in regime permanent THD	5.3 %	1.68 %
Frequency of switching	Good	High
Response time	Medium	Fast
Error	Medium	Low
Complexity of implantation	High	Low

VII. CONCLUSIONS

This work describes the modelling and the design of a DFIG-based wind energy conversion system using model predictive current control 3L-NPC inverter with hysteresis current control of DC voltage rectifier under variable wind speed.

The results of the simulation of this smart current predictive control showed high performance and dynamic behaviour even at high power. Also, the measured DC voltage closely follows the reference voltage and this proves its robustness, with a very low total harmonic distortion of the currents at the output of the inverter 3L-NPC (THD % = 1.68 %).

The optimisation techniques with metaheuristic algorithms

are more accurate for THD optimisation and switching loss reduction.

Future work will focus on the experimental validation: using DC machine for creating mechanical speed of the turbine, multiplier, doubly-fed induction generator, PWM rectifier, board Dspace1104, current sensors, voltage sensors, DC voltage stabiliser, control interface, inverter three-level-NPC, MATLAB/Simulink and control Desk.

APPENDIX A

TABLE A-I. PARAMETERS.

DFIG parameters	Turbine parameters
Pn = 1.5 Mw Vs = 220 V f = 50 Hz RS = 3.82 mΩ Rr = 2.97 Mω LS = 12.241 mH Lr = 12.241 mH M = 12.12 mH J = 256 kg.m2 F = 0 N.m/s P = 2	R = 40 m J = 256 kg.m^2 G = 70

CONFLICTS OF INTEREST

The authors declare that they have no conflicts of interest.

REFERENCES

[1] P. Huynh, A. J. Samarakoon, K. S. Haran, and A. Banerjee, "Winding layout considerations for an integrated generator–rectifier system", *IEEE Transactions on Power Electronics*, vol. 37, no. 2, pp. 2352–2361, 2022. DOI: 10.1109/TPEL.2021.3107546.

[2] M. Arif, M. Shahzad, J. Saleem, W. Malik, and A. Majid, "Conversion stage three port high gain converter for PV integration with DC microgrid", *Elektronika ir Elektrotechnika*, vol. 26, no. 3, pp. 69–78, 2020. DOI: 10.5755/j01.eie.26.3.25763.

[3] H. Bhattacherjee, D. Mukherjee, and C. Chakraborty, "Three-level Vienna rectifier with a brushless and permanent magnetless generator for wind energy conversion systems", *Power Electronics and Drives*, vol. 7, no. 42, pp. 84–102, 2022. DOI: 10.2478/pead-2022-0007.

[4] S. Choudhury, M. Bajaj, T. Dash, S. Kamel, and F. Jurado, "Multilevel inverter: A survey on classical and advanced topologies, control schemes, applications to power system and future prospects", *Energies*, vol. 14, no. 18, p. 5773, 2021. DOI: 10.3390/en14185773.

[5] G. K. Devineni and A. Ganesh, "Problem formulations, solving strategies, implementation methods & applications of selective harmonic elimination for multilevel converters", *Journal Européen des Systèmes Automatisés*, vol. 53, no. 6, pp. 939–952, 2020. DOI: 10.18280/jesa.530620.

[6] H. Eroğlu, E. Cuce, P. M. Cuce, F. Gul, and A. Iskenderoğlu, "Harmonic problems in renewable and sustainable energy systems: A comprehensive review", *Sustainable Energy Technologies and Assessments*, vol. 48, art. 101566, pp. 1–20, 2021. DOI: 10.1016/j.seta.2021.101566.

[7] R. Sarker, A. Datta, and S. Debnath, "FPGA-based high-definition SPWM generation with harmonic mitigation property for voltage source inverter applications", *IEEE Transactions on Industrial Informatics*, vol. 17, no. 2, pp. 1352–1362, 2021. DOI: 10.1109/TII.2020.2983844.

[8] V. Jayakumar, B. Chokkalingam, and J. L. Munda, "A comprehensive review on Space Vector Modulation techniques for Neutral Point Clamped Multi-Level Inverters", *IEEE Access*, vol. 9, pp. 112104–112144, 2021. DOI: 10.1109/ACCESS.2021.3100346.

[9] M. Wu, Y. W. Li, and G. Konstantinou, "A comprehensive review of capacitor voltage balancing strategies for multilevel converters under selective harmonic elimination PWM", *IEEE Transactions on Power Electronics*, vol. 36, no. 3, pp. 2748–2767, 2021. DOI: 10.1109/TPEL.2020.3012915.

[10] M. M. A. Alakkad, Z. Rasin, M. Rasheed, W. Abd Halim, and R. Omar, "Real-time switching thirteen-level modified CHB-Multilevel inverter using artificial neural network technique based on selective harmonic elimination", *Indonesian Journal of Electrical Engineering and Computer Science*, vol. 20, no. 3, pp. 1642–1652, 2020. DOI: 10.11591/ijeecs.v20.i3.pp1642-1652.

[11] R. Palanisamy, T. M. Thamizh Thentral, M. Ramesh, A. Rajkumar, and K. Vijayakumar, "Implementation of four dimensional space vector modulation for five phase voltage source inverter", *Ain Shams Engineering Journal*, vol. 12, no. 3, pp. 2891–2898, 2021. DOI: 10.1016/j.asej.2020.12.017.

[12] I. Sami, S. Ullah, Z. Ali, N. Ullah, and J.-S. Ro, "A super twisting fractional order terminal sliding mode control for DFIG-based wind energy conversion system", *Energies*, vol. 13, no. 9, p. 2158, 2020. DOI: 10.3390/en13092158.

[13] E. H. Dursun and A. A. Kulaksiz, "Second-order fast terminal sliding mode control for MPPT of PMSG-based wind energy conversion system", *Elektronika ir Elektrotechnika*, vol. 26, no. 4, pp. 39–45, 2020. DOI: 10.5755/j01.eie.26.4.25762.

[14] S. Gao, H. Zhao, Y. Gui, D. Zhou, and F. Blaabjerg, "An improved direct power control for doubly fed induction generator", *IEEE Transactions on Power Electronics*, vol. 36, no. 4, pp. 4672–4685, 2021. DOI: 10.1109/TPEL.2020.3024620.

[15] R. Cheikh, B. Boualem, and H. Belmili, "Improved Fuzzy Logic MPPT Controller of Stand-alone WECS-based PMSG under stochastic wind environment", *J. Ren. Energies*, vol. 1, no. 1, pp. 31–42, 2023. DOI: 10.54966/jreen.v1i1.1096.

[16] H. Acikgoz, C. Yildiz, R. Coteli, and B. Dandil, "DC-link voltage control of three-phase PWM rectifier by using artificial bee colony based type-2 fuzzy neural network", *Microprocessors and Microsystems*, art. 103250, pp. 1–13, 2020. DOI: 10.1016/j.micpro.2020.103250.

[17] A. Babu, B. G. Shivaleelavathi, and V. Yatnalli, "Efficiency analysis and design considerations of a hysteretic current controlled parallel hybrid Envelope Tracking Power Supply", *Engineering, Technology & Applied Science Research*, vol. 13, no. 1, pp. 9812–9818, 2023. DOI: 10.48084/etasr.5414.

[18] M. Malinowski, "Sensorless control strategies for three-phase PWM rectifiers", Ph.D. dissertation, Faculty of Electrical Engineering Institute of Control and Industrial Electronics, Warsaw University of Technology, 2001. DOI: 10.1016/B978-012402772-5/50012-0.

[19] J. Ren, Y. Sun, S. Zhang, S. Zhang, Y. Liu, K. Li, and X. Jiang, "A novel self-powered smart current sensor for power equipment", *Elektronika ir Elektrotechnika*, vol. 25, no. 2, pp. 20–27, 2019. DOI: 10.5755/j01.eie.25.2.23199.

[20] Q. Deng, B. Gou, X. Ge, C. Lin, D. Xie, and X. Feng, "A high-accuracy-light-AI data-driven diagnosis method for open-circuit faults in single-phase PWM rectifiers", *IEEE Transactions on Transportation Electrification*, vol. 9, no. 3, pp. 4352–4365, 2023. DOI: 10.1109/TTE.2023.3238009.

[21] F. Kendouli, K. Nabti, and K. Abed et H. Benalla, "Modélisation, simulation et contrôle d'une turbine éolienne à vitesse variable basée sur la génératrice asynchrone à double alimentation", *Revue des Energies Renouvelables*, vol. 14, no. 1, pp. 109–120, 2011. DOI : 10.54966/jreen.v14i1.245.

[22] Z. Zhou, J. Son, Y. Yu, Q. Xu, and X. Zhou, "Research on high-quality control technology for three-phase PWM rectifier", *Electronics*, vol. 12, no. 11, p. 2417, 2023. DOI: 10.3390/electronics12112417.

[23] T. Abdelkrim, E. M. Berkouk, T. Benslimane, and K. Benamrane, "Feedback control of three-level PWM rectifier: Application to the stabilization of DC voltages of five-level NPC active power filter", *Archives of Control Sciences*, vol. 20, no. 3, pp. 317–339, 2010. DOI: 10.2478/v10170-010-0020-9.

[24] E.-S. Jun, M. H. Nguyen, and S.-S. Kwak, "Model predictive control method with NP voltage balance by offset voltage injection for three-phase three-level NPC inverter", *IEEE Access*, vol. 8, pp. 172175–172195, 2020. DOI: 10.1109/access.2020.3024634.

[25] J. S. Artal-Sevil, J. M. Lujano-Rojas, C. Bernal-Ruiz, and I. S. Gorrachategui, "Analysis of power losses in a three-phase inverter 3L-NPC. Comparison with different PWM modulation techniques", in *Proc. of 2018 XIII Technologies Applied to Electronics Teaching Conference (TAEE)*, 2018, pp. 1–9. DOI: 10.1109/TAEE.2018.8476107.

[26] F. Guo, Z. Ma, F. Diao, Y. Zhao, and P. Wheeler, "Hybrid virtual coordinate-driven CBPWM strategy of three-level T-type NPC converters for electric aircraft propulsion applications", *IEEE Transactions on Industrial Electronics*, vol. 71, no. 3, pp. 2309–2319, 2024. DOI: 10.1109/TIE.2023.3266552.

[27] A. K. Bonala, S. R. Sandepudi, and V. P. Muddineni, "Model predictive current control with modified synchronous detection technique for three-phase 3L-NPC multi-functional solar photovoltaic system", in *Proc. 2016 IEEE International Conference on Power Electronics, Drives and Energy Systems (PEDES)*, 2016, pp. 1–6. DOI:

10.1109/PEDES.2016.7914309.

[28] J. Rodriguez *et al.*, "Predictive current control of a voltage source inverter", *IEEE Transactions on Industrial Electronics*, vol. 54, no. 1, pp. 495–503, 2007. DOI: 10.1109/TIE.2006.888802.

[29] D. Rojas, M. Rivera, J. Muñoz, C. Baier, and P. Wheeler, "Predictive current control applied to a 3L-NPC inverter", in *Proc. of 2021 IEEE International Conference on Automation/XXIV Congress of the Chilean Association of Automatic Control (ICA-ACCA)*, 2021, pp. 1–7. DOI: 10.1109/ICAACCA51523.2021.9465309.

[30] Q. Wang *et al.*, "A low-complexity optimal switching time-modulated model-predictive control for PMSM with three-level NPC converter", *IEEE Transactions on Transportation Electrification*, vol. 6, no. 3, pp. 1188–1198, 2020. DOI: 10.1109/TTE.2020.3012352.

[31] A. Katkout, T. Nasser, and A. Essadki, "An efficient model predictive current control algorithm for grid-connected multi-level inverter with computational delay compensation", in *Proc. of 2020 International Conference on Electrical and Information Technologies (ICEIT)*, 2020, pp. 1–6. DOI: 10.1109/ICEIT48248.2020.9113234.